ELSEVIER

Colloids and Surfaces
A: Physicochemical and Engineering Aspects 140 (1998) 177–182

COLLOIDS AND SURFACES A

Electrochemical impedance spectroscopy analysis of chalcopyrite $CuFeS_2$ electrodes

P. Velásquez [a], H. Gómez [a], D. Leinen [b], J.R. Ramos-Barrado [b,*]

[a] *Instituto de Química, Universidad Católica de Valparaiso, Casilla 4059, Valparaiso, Chile*
[b] *Departemento de Física Aplicada, Facultad de Ciencias, Universidad de Málaga, E-29071 Málaga, Spain*

Received 10 February 1997; accepted 27 May 1997

Abstract

A chalcopyrite $CuFeS_2$ electrode obtained from the "El Teniente" mine has been studied by Electrochemical Impedance Spectroscopy (EIS) in an alkaline solution for different oxidation potentials. The experimental results can be interpreted from a Randles equivalent circuit, $V_{dc} < 0.4$ V vs. saturated calomel electrode (SCE), and a surface

Keywords: Electrochemical Impedance Spectroscopy (EIS); Chalcopyrite; $CuFeS_2$; Electrode

1. Introduction

The industrial flotation process of chalcopyrite $CuFeS_2$ produces a number of irreversible degradation processes such as redox reactions, adsorption and others which affect the mineral surface and a layer of modified mineral is grown; these changes modify the hydrophobicity of mineral and the industrial performance of the flotation process [1,2]. A number of studies [3] have shown that, in general, these films consist of two layers; an inner barrier layer consisting of a disordered crystalline phase which is typically 0.5–2 nm thick and an outer hydrated layer which may extend to significant distances from the surfaces depending upon the system under study; this layer implies a strong change of impedance and capacity electrode and the electrode/electrolyte interface.

The object in Electrochemical Impedance Spectroscopy (EIS) is to correlate features of impedance spectra with their underlying microstructural origins by means of appropriate and reasonable equivalent circuit. Analysis of experimental data of EIS provides information about physical and chemical processes present in the electrode/electrolyte interface, such as charge transfer resistance, which is related to the faradaic current flowing across the interface, and the Warburg impedance, which is related to the diffusion-controlled migration.

The aim of this paper is the application of EIS to a chalcopyrite electrode in an alkaline solution of borate (pH 9.2) in order to determine its equivalent electrochemical circuit and the influence of applied potential in the behaviour of electrode/electrolyte interface. Because these processes are charge transfer processes, EIS is very valuable because of its ability, in a single experiment, to

* Corresponding author.

PII S0927-7757(97)00276-8

detect interface and bulk relaxation covering a wide range of relaxation times [4,5].

2. Experimental

The working electrode is natural chalcopyrite ($CuFeS_2$) from the "El Teniente" mine (Chile); its crystalline structure has been determined by X-ray diffraction. The sample was placed on epoxy resin. The area of the electrode exposed to the electrolyte was 0.2 cm^2. The electrode was attached to a copper wire with In–Ga. The auxiliary electrode was made of graphite and the reference electrode was a saturated calomel electrode (SCE). Before each measurement a fresh electrode surface was prepared by wet abrading with 600 grade silicon carbide paper and then rinsing with deoxygenated deionized water. Finally, a fine polish was achieved with alumina suspension of first 0.3 and then 0.05 m particle size. The electrolyte solution was prepared with disodium tetraborate decahydrate GR (borax) from Merck (EWG-Nr. 215-540-4) to 0.05 M in deoxygenated deionized and, by heat treatment, dicarbonated water obtaining a constant ionic strength of 0.2 at pH 9.2. Impedance data were recorded with a Solartron 1255 Frequency Response Analyzer. For all impedance measurements, the Solartron sine wave output was superimposed on an applied d.c. bias from a Solartron 1286 Electrochemical Interface. The FRA and the EI were both controlled by computer by means of an "ad hoc" handmade program. Measurements were made for the frequency range from 10 mHz to 10 kHz for different d.c. applied potential (−0.1 V to +0.7 V vs. SCE) and a.c. potential of 0.01 V [6]. The d.c. potential range is from that corresponding to the natural state (−0.1 V vs. SCE) to that corresponding to the beginning of compositional change in the $CuFeS_2$ electrode surface by an oxidation process (+0.8 V vs. SCE). Before each EIS measurement, the d.c. potential is applied by a potentiostat in the positive sweep direction (PSD) from −0.1 V vs. SCE to the value of the applied d.c. potential with a sweep rate of 5 mV/s.

3. Experimental results

Data directly measured as complex impedance Z^* were converted into complex capacitance C^* using the relation [7,8]:

$$C^*(\omega) = \frac{1}{(j\omega Z^*)}$$

which is related to the complex dielectric constant through the relation:

$$\epsilon^*(\omega) = \frac{C^*}{C_0}$$

where C_0 is the vacuum capacitance and $j = \sqrt{(-1)}$.

3.1. Impedance

Fig. 1(a)–(d) presents the real (horizontal, Z') and imaginary (vertical, Z'') components in the complex plane of the total circuit impedance for each frequency and different applied potentials. At high frequencies, the data show a semicircle followed, at intermediate and low frequencies, by a straight line of slope 45°. As the applied potential is moved to more positive values, the semicircle at high frequencies increases progressively and presents a dramatic change for potential values higher than 0.4 V vs. SCE. Figs. 2 and 3 show the impedance modulus and phase angle Bode plot.

3.2. Differential capacitance

Variations of the real part of the complex capacitance:

$$\log C = \log\left(\frac{1}{2\pi f \,\mathrm{Im}(Z) A}\right)$$

for some d.c. potential are plotted in Fig. 4(a), where A is the apparent electrode area, $\mathrm{Im}(Z)$ the imaginary part of Z^* and f the frequency [9]. Fig. 4(b) shows the capacitance complex plot for some d.c. potential. For an ideal capacitance, which is an independent frequency capacitance, the variation of $\log C$ with $\log f$ is a horizontal straight line [10]. This capacitance is a "frequency-

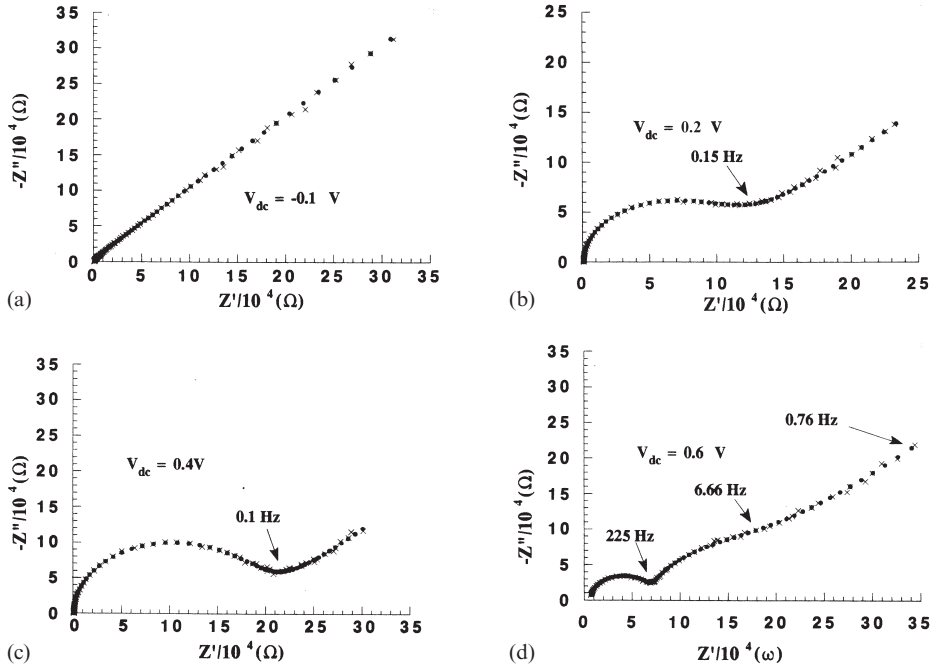

Fig. 1. Nyquist plot of complex impedance for some V_{dc} vs. SCE: (a) −0.1 V; (b) +0.2 V; (c) +0.4 V; (d) +0.6 V.

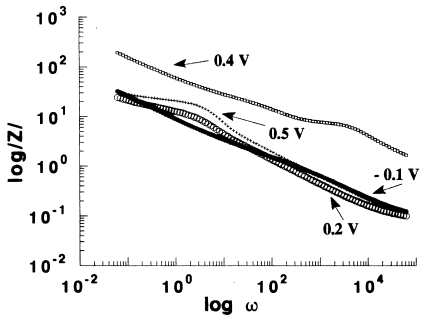

Fig. 2. Impedance modulus plot vs. frequency for some V_{dc} vs. SCE: ●, −0.1 V; ○, +0.2 V; □, +0.4 V; +, +0.5 V.

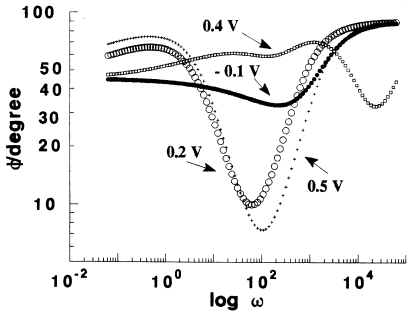

Fig. 3. Phase angle plot vs. frequency for some V_{dc} vs. SCE: ●, −0.1 V; ○, +0.2 V; □, +0.4 V; +, +0.5 V.

dependent'' capacitance rather than an ''ideal'' capacitance. This effect is usually called frequency dispersion of capacitance or simply capacitance dispersion. Experimental variations of log C are linear with a low slope at each end of the frequency domain. This may be explained by an empirical constant phase element (CPE) with $Q=1/Kp^n$. In this expression, n is a dimensionless number, lower but close to 1, K is a constant whose dimension is F s^{n-1} and $p=j\omega$ with $\omega=2\pi f$. Q is equivalent to the impedance of a capacitance $C=K(2\pi f)^{n-1}$, or $\log C=\log[K(2\pi)^{n-1}]+(n-1)\log f=\text{constant}(n-1)\log f$, that is, the CPE behaves as a capacitance varying with the frequency. This modification to an ideal capacitance behaviour has already been explained by distribution effects [11], porosity [12] or fractal geometry [13].

One may distinguish in Fig. 4(a) and (b) three kinds of frequency domain in which slopes differ for each d.c. applied potential, moreover, the Mott–Schottky plot shows a dramatic change

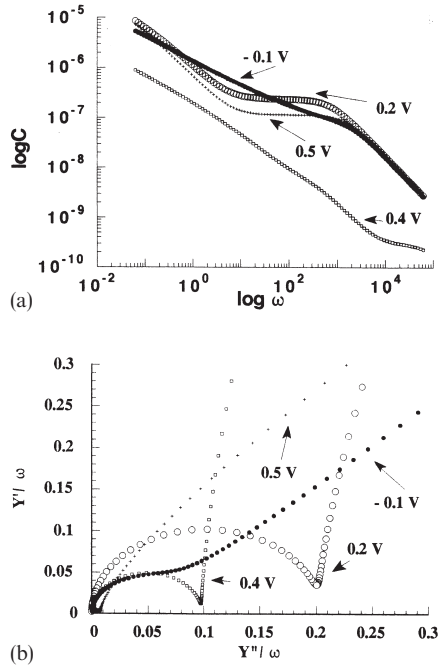

Fig. 4. (a) Complex capacitance modulus vs. frequency for some V_{dc} vs. SCE: ●, −0.1 V; ○, +0.2 V; □, +0.4 V; +, +0.5 V. (b) Nyquist plot of complex capacitance for some V_{dc} vs. SCE: ●, −0.1 V; ○, +0.2 V; □, +0.4 V; +, +0.5 V.

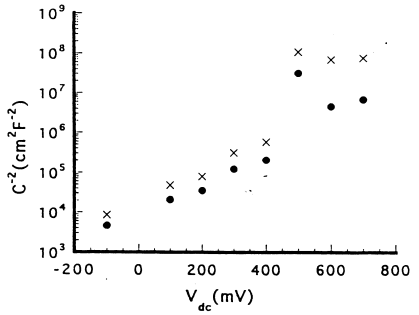

Fig. 5. Mott–Schottky plot: ●, 100 Hz; ×, 1 kHz.

when $V_{dc} > 0.4$ V vs. SCE (Fig. 5); for a V_{dc} lower than 0.4 V vs. SCE C^{-2} it presents an exponential increase which is almost independent of frequency and implies an n-type semiconductor.

3.3. Equivalent circuit

The above results can be represented by a simple equivalent R–C circuit of the type illustrated in Fig. 1(a) (Randles circuit) [14]. In such a circuit, R_e represents the resistance of the electrolyte between the electrode under study and the counter-electrode and others ohmic resistance, that is, the uncompensated resistance; R_i is the interfacial resistance and/or the charge transfer resistance; C_{dl} is the double layer capacitance, and W is a Warburg element, which takes into account diffusion effects [15]. In the Nyquist plot, going from high to low frequencies, the semicircle corresponding to the R_i–C_{dl} parallel combination and the straight line is due to diffusion impedance. The experimental data were fitted by means of a non-linear least squares method [16] (Table 1). For $V_{dc} > 0.5$ V vs. SCE the plots show a new relaxation process and the experimental data can be modeled by a surface layer equivalent circuit [17], Fig. 6(b); in this circuit R_{sl} is the surface layer resistance, C_{sl} the polarization of surface layer, R_{ct} the charge transfer resistance, W a Warburg impedance, the serial $R_{ct}W$ association represents the faradaic current branch and the $W'C_{dl}$ association is the non-faradaic current one originated by the displacement current due to charge polarization. The existence of a surface layer modifies the double layer capacitance, which is associated with the mobile species in the surface layer. Since the double layer is confined to a small fraction of the surface layer, the relation $C_{dl} > C_{sl}$ can be anticipated, so we are justified in putting the surface layer circuit in series with the interfacial region circuit.

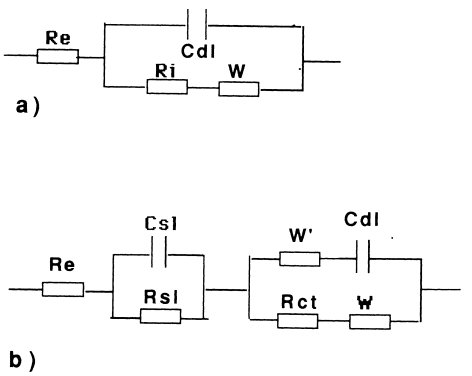

Fig. 6. (a) Randles circuit; (b) surface layer circuit.

Table 1
Characteristic parameters for Randles and surface layer circuit

V_{dc} vs. SCE	R_i (kΩ)	C_{dl} (μF cm^{-2})	W (10^{-6} Ω^{-1} Hz$^{1/2}$)	R_{sl} (kΩ)	C_{sl} (μF cm^{-2})	R_{ct} (kΩ)
-0.1	19.79	0.63	8.9			
0.1	45	2.1	20.7			
0.2	10	1.63	20.8			
0.3	16.22	1.03	23.5			
0.4	18.69	0.8	24.1			
0.5	25.55	0.058	1.87			
0.6		0.062	1.58	61.93	0.0023	10.5
0.7		0.15	1.21	41.86	0.0085	83.7

4. Discussion

According to the thermodynamic diagram [18], chalcopyrite electro-oxidation at pH 9.2 must show the following general process:

$CuFeS_2 \rightarrow Fe_2O_3 \rightarrow CuS \rightarrow CuFeO_2 \rightarrow CuO$,
S, Fe_2O_3

and the variation in modulus of complex impedance, ($|Z^*| = \sqrt{Z'^2 + Z''^2}$) and the real part of the complex capacitance must be due to the formation of a layer of these species. The slow change of Randles elements and other electrochemical characteristic parameters, impedance, capacitance and C^{-2}, implies a slow growth of the oxide layer. From XPS, voltammogram and photovoltammogram data in the positive sweep direction [6,19], we can assume that for potentials lower than 0.4 V vs. SCE a thin layer of Fe_2O_3 is formed by the Fe^{3+} ion migration to the surface electrode; but Cu and S are not oxidized. However, the strong change for potentials higher than 0.4 V vs. SCE implies quick modification of the layer and film/electrolyte interface. The charge transfer resistance presents the most important transformation; for $V_{dc} < 0.4$ V vs. SCE, a layer of $CuFe_{1-x}S_2$ is grown over the electrode surface, by means of the formation of a metastable compound (CuS_2^*) and the migration of Fe^{3+} ions; however, for $V_{dc} > 0.4$ V vs. SCE, there is a migration of Fe^{3+} ions and S atoms to give rise to the formation of Fe_2O_3 and CuO from a deeper layer whilst elemental S is deposited on the electrode surface and the development of non-homogeneous films on the surface of the electrode is originated. The change of surface composition implies a change of the equivalent circuit; now, it is necessary to take into account the new relaxation due to a surface layer electrolyte which is produced by the oxidized surface of the electrode; moreover, the new composition of surface layer implies a non-faradaic current due to a strong change of the charge polarization.

The increase of interfacial resistance R_i with the applied potential for the range $V_{dc} > 0.4$ V vs. SCE can be attributed to an increase of film thickness, and the strong decrease for $V_{dc} > 0.4$ V vs. SCE implies a change of surface composition with a better electrical conductivity. The Warburg element of the Randles circuit presents a slow increase when the potential moves into more positive values ($V_{dc} < 0.4$ V vs. SCE); as this circuit element is inversely proportional to the diffusion coefficient, this result indicates that the charge carrier mobility changes with the applied potential, and more specifically, in agreement with the kinetics of the process which become increasingly diffusion-controlled; moreover, the strong decrease for $V_{dc} > 0.4$ V vs. SCE implies an increase in the diffusion coefficient when there is CuO on the electrode surface.

5. Conclusion

The oxidation of chalcopyrite in an alkaline solution produces a modification of the electrode surface; for values lower than 0.4 V vs. SCE a Randles equivalent circuit can be used, but the Nyquist plots present a change when the applied potential is higher than 0.4 V vs. SCE and a surface

layer model must be used. This change gives rise to a modification of the charge transfer resistance and the diffusion coefficient of charge carriers across the interlayer electrode/electrolyte resistance. This behaviour is due to the initial formation of a layer of Fe_2O_3 and an inner layer of CuO and Fe_2O_3 which confer an irregular and non-homogeneous surface to the electrode.

References

[1] A.N. Buckley, Colloids and Surfaces A 93 (1994) 159.
[2] D.P. Tao, Y.Q. Li, P.E. Richardson, R.H. Yoon, Colloids and Surfaces A 93 (1994) 229.
[3] D.D. Macdonald, S.I. Smeldley, Electroanal. Acta 35 (1990) 1956.
[4] S.J. Lenhart, D.D. Macdonald, B.G. Pound, J. Electrochem. Sci. 135 (1988) 1063.
[5] S.D. Bhakta, D.D. Macdonald, B.J. Pound, M. Urquidi-Macdonald, J. Electrochem. Soc. 138 (1991) 1353.
[6] H. Gómez, R. Schribler, R. Córdova, J. Casanova, P. Velásquez, Estudio fotoelectroquimico de la calcopirita ($CuFeS_2$) en medio alcalino.
[7] J.R. Macdonald, Impedance Spectroscopy Analysis, John Wiley and Sons, New York, 1987.
[8] M.A. Alin, in: R.A. Gerhardt, S.R. Taylor and E.J. Garboczi (Eds.), Electrically Based Microstructural Characterization, Material Research Society, Pittsburgh, PA, 1996.
[9] G. Barral, F. Njanjo-Eyoke, S. Maximovitch, Electrochim. Acta 40 (1995) 2815.
[10] J. Jonscher, Dielectric Relaxation in Solids, Chelsea Dielectric Press, UK, 1983.
[11] G.J. Brug, A.L.G. Van Den Eeden, M. Sluyters-Rehbach, J.H. Sluyters, J. Electroanal. Chem. 176 (1984) 275.
[12] L.M. Gassa, J.R. Vilche, M. Ebert, K. Jüttner, W.J. Lorenz, J. Appl. Electrochem. 20 (1990) 677.
[13] T. Pajkossy, L. Nyikos, Electrochim. Acta 34 (1989) 171.
[14] J.E.B. Randles, Discuss. Faraday Soc. 1 (1947) 11.
[15] E. Warburg, Ann. Physik 67 (1899) 493.
[16] B.A. Boukamp, Solid State Ionics 20 (1986) 31.
[17] M.G.S.R. Thomas, P.G. Bruce, J.B. Goodenough, J. Electrochem. Soc. 132 (1986) 1521.
[18] F.W.H. Dean, G.H. Kelsall, in: Proc. Int. Symp. on Electrochemistry in Mineral and Metal Processing III, Electrochemical Society, Pennington, NJ, 1994, p. 297.
[19] P. Velásquez, H. Gòmez, J.R. Ramos-Barrado, D. Leinen, Colloids and Surfaces, in Press